Talanta 115 (2013) 24–31

Contents lists available at ScienceDirect

Talanta

journal homepage: www.elsevier.com/locate/talanta

Biopolymer capped silver nanoparticles as fluorophore for ultrasensitive and selective determination of malathion

N. Vasimalai, S. Abraham John *

Centre for Nanoscience and Nanotechnology, Department of Chemistry, Gandhigram Rural Institute, Gandhigram, 624302 Dindigul, Tamilnadu, India

ARTICLE INFO

Article history:
Received 12 January 2013
Received in revised form
5 April 2013
Accepted 12 April 2013
Available online 19 April 2013

Keywords:
Malathion
Silver nanoparticles
Chitosan
Fluorescence quenching
Pesticide

ABSTRACT

This paper describes a novel luminescent sensor for malathion using chitosan capped silver nanoparticles (Chi-AgNPs) as fluorophore. The Chi-AgNPs were synthesized by the wet-chemical method and were characterized by absorption, fluorescence, HR-TEM, XRD and DLS techniques. The Chi-AgNPs show the absorption maximum at 394 nm and emission maximum at 536 nm. While adding 10 μM malathion, yellow color Chi-AgNPs was changed to brown and the absorbance was decreased along with a redshift. The observed spectral and color changes were mainly due to the aggregation of Chi-AgNPs. This was confirmed by zeta potential, DLS and HR-TEM studies. No significant absorption spectral change was observed for Chi-AgNPs in the presence of less than micromolar concentrations of malathion. However, the emission intensity of Chi-AgNPs was decreased and the emission maximum was shifted toward higher wavelength in the presence of picomolar concentration of malathion. Based on the decrease in emission intensity, the concentration of malathion was determined. The Stern–Volmer constant, Gibbs free energy change, association constant, quantum yield and binding constant were calculated and the quenching mechanism was proposed. The Chi-AgNPs show good selectivity toward the determination of 10 nM malathion in the presence of 1000-fold higher concentrations of common interferents. A good linearity was observed for the emission intensity against 1×10^{-9}–10×10^{-12} M malathion and the detection limit was found to be 94 fM L^{-1} ($S/N=3$). The proposed method was successfully applied to determine malathion in fruits and water samples and the obtained results were validated with HPLC.

1. Introduction

The pesticides assisted to extensively reduce crop losses and to improve the yield of crops such as corn, maize, vegetables, potatoes and cotton [1–3]. Worldwide use of pesticides increased terrifically since the 1960s [3]. Although pesticides are beneficial they adversely affect both the environment and human health. Residues of pesticides pollute the soil and water, persist in the crops and enter the food chain and are finally swallowed by human with foodstuffs and water. Further, pesticides were responsible for contributing to biodiversity losses and deterioration of natural habitats [4–6].

Malathion is an organophosphorous pesticide which is extensively applied on crops like banana, citrus fruits, tobacco and on vegetable crops like tomato, beans, brinjal and carrot. It can control the pests like aphids and similar sap-sucking insects, various weevils, small beetles, scale insects and red spider mites [7–9]. Very recently, in one of the southern states of India, Tamilnadu, 5367 people were affected by dengue fever and about 39 were died [10]. Indian government is making a lot of efforts to control the mosquitoes. Malathion is very widely used in urban centers as a fog against mosquitoes by the public health authorities in India [7–10]. Moreover, it is also used to control animal ectoparasite and human body lice [11].

The acute toxicity of malathion to animals is caused by inhibition of acetylcholinesterase (AChE), an important enzyme functioning to hydrolyze the neurotransmitter acetylcholine (ACh) [8]. The inactivation of AChE causes an over accumulation of ACh and thereby disrupts the nerve transmissions [9]. The genotoxic studies indicate that malathion can also induce DNA damage [12]. Malathion has also been shown to modulate oxidative stress and cholinesterase depression in saliva and plasma and increase plasma glucose concentration associated with stimulation of hepatic glycogen phosphorylase and phosphoenolpyruvate carboxykinase in rats [12]. Toxic symptoms resulting from human exposure to malathion, include breathing problems, headache, nausea and dizziness, while high exposure can produce fetal poisoning [13]. Malathion can persist in the human body for at least two generations [10]. It is suspected to cause kidney problems, human birth defects and child leukemia [11]. Due to its extensive application, it finds its way into surface water bodies through agricultural runoff and municipal waste water. Hence, it is

* Corresponding author. Tel.: +91 451 245 2371; fax: +91 451 245 3031.
E-mail address: abrajohn@yahoo.co.in (S. Abraham John).

0039-9140/$ - see front matter © 2013 Elsevier B.V. All rights reserved.
http://dx.doi.org/10.1016/j.talanta.2013.04.033

necessary to determine the residues of malathion in water and vegetables to protect the human beings and environment from its hazardous effect.

Generally, malathion was determined by high performance liquid chromatography [14], gas chromatography coupled with mass spectrometry [15], voltammetry [16], infra-red spectroscopy [17] and Raman spectrometry [18]. Among these methods, many of them are time consuming and labor-intensive due to the complex pretreatment, require expensive instrumentation and high cost of personnel and are not readily adaptable to on-site detection [14,15,17,18]. Therefore, it is essential to develop a simple, rapid, low cost and field-portable method for the detection of malathion in environmental samples. In recent years, the determination of toxic chemicals by the spectrofluorimetry method has received much attention [19–22] because of its high sensitivity, selectivity, reproducibility, less time consumption and simple experimental conditions [23–25]. Recently, metal nanoparticles based pesticides sensors have been gaining momentum due to their interesting optical, catalytic and electrical properties [4,5,9,25]. Among the different metallic nanoparticles, silver nanoparticles (AgNPs) show excellent optical properties, good conductivity, chemical stability and catalytic activity [26–28]. The AgNPs have been used extensively as an antibacterial agent, food storage, textile coatings and toxic chemicals sensor [26–29].

Chitosan is a degradable biopolymer (Chart 1) and it has several attractive properties including excellent film forming ability, high permeability toward water, good adhesion, non-toxicity and biocompatibility [30–32]. The derivatives of chitosan have been applied for the removal of various heavy metal ions from aqueous solution [33]. Therefore, we have used chitosan as a capping agent for the synthesis of AgNPs in the present study. The present work describes the luminescent sensor for malathion using chitosan capped silver nanoparticles (Chi-AgNPs) as fluorophore. The Chi-AgNPs show the absorption maximum at 394 nm and the emission maximum at 536 nm while exciting at 394 nm. The emission intensity of Chi-AgNPs was decreased and the emission maximum was shifted to higher wavelength while adding picomolar malathion. Based on the decrease in emission intensity, we have determined the concentration of malathion. The lowest detection limit was found to be 94 fM L^{-1}. The obtained results were validated with HPLC.

2. Experimental

2.1. Chemicals

Silver nitrate, malathion and acetic acid were purchased from Sigma-Aldrich. Sodium borohydride ($NaBH_4$) was obtained from Merck (India). Chitosan with its deacetylation degree of 85% was purchased from Pelican Biotech and Chemicals Labs, Kerala (India). All other chemicals used in this investigation were of analytical grade and used directly without further purification. Millipore Milli-Q (18 MΩ cm) water was used in all the experiments.

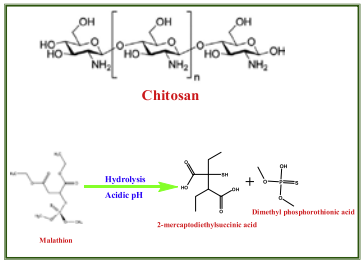

Chart 1. Structure of chitosan and hydrolysis of malathion in acidic pH.

2.2. Instrumentation

The high resolution transmission electron microscopy (HR-TEM) images of AgNPs were obtained from a JEOL JEM 2100 Advanced Analytical HR-TEM, operating at 200 kV. For TEM measurements, the sample was prepared by dropping 2 μL of a colloidal solution onto a carbon-coated copper grid. UV–visible spectral measurements were performed on a JASCO V-550 UV–visible spectrophotometer. Fluorescence spectra were measured by using a JASCO FP-6500 spectrofluorimeter equipped with a Xenon discharge lamp, and 1 cm quartz cell at room temperature (about at 298 K). A larger volume (500 mL) of Chi-AgNPs was synthesized and the particles were separated by centrifuging at 10,000 rpm and repeatedly washed with water and dried in vacuum. The dried AgNPs powder was used for X-ray diffraction (XRD) analysis. XRD analysis was carried out with a Rigaku X-ray diffraction unit using Ni-filtered Cu Kα ($\lambda = 1.5406$) radiation. Dynamic light scattering (DLS) and zeta potential measurements were performed on Zetasizer Nano S90 (Malvern). Millipore Milli-Q (18 MΩ cm) water was prepared by using Direct-Q Millipore (Cylus Laboratory Equipment, France).

2.3. Synthesis of Chi-AgNPs

All glasswares were thoroughly cleaned with freshly prepared aquaregia (3:1; HCl/HNO_3) and rinsed comprehensively with Millipore water prior to use. The colloidal solution of chitosan capped AgNPs was prepared as follows. 5 mL of $AgNO_3$ (7 mM) and 1 mL of 1% chitosan in acetic acid were added to 86 mL of water in a round bottom flask with constant stirring. To this solution, 8 mL of 0.05 M $NaBH_4$ was added and the color of the solution turns into yellow immediately after the final addition, indicating the formation of AgNPs. The stirring was continued for another 30 min. The synthesized Chi-AgNPs were purified by centrifugation at 10,000 rpm and then the filtrate was dissolved in Millipore water. The purified Chi-AgNPs were used for further studies.

2.4. Real sample analysis

A typical spectrofluorimetric analysis of malathion in polluted lake water and fruit samples was achieved as follows. The mangos and grapes were chosen as the spiked sample to evaluate malathion residues in actual fruits using the Chi-AgNPs. The different concentrations of malathion were sprayed onto mangos and grapes by an atomizer. After 3 days at room temperature, the edible parts of the fruits were taken and crushed well. From the crushed mangos or grapes, 10 g was mixed with 50 mL water in a 100 mL flask and shaken vigorously for 30 min. Then, insoluble draff was removed by a simple filtration. A control sample was also prepared by using the same procedure.

3. Results and discussion

3.1. Spectral studies of chitosan in the presence of malathion

The UV–visible spectrum of chitosan is shown in Fig. 1a (inset). It shows a shoulder band around 210 nm. Fig. S1 (Supporting information) shows the UV–visible spectra of chitosan in the presence of different concentrations of malathion. The absorbance around 210 nm was decreased after the addition of 100 μM malathion. Further increasing the concentration of malathion, the absorbance around 210 nm was dramatically decreased. No significant decrease in absorbance at 210 nm was observed in the presence of less than 100 μM malathion.

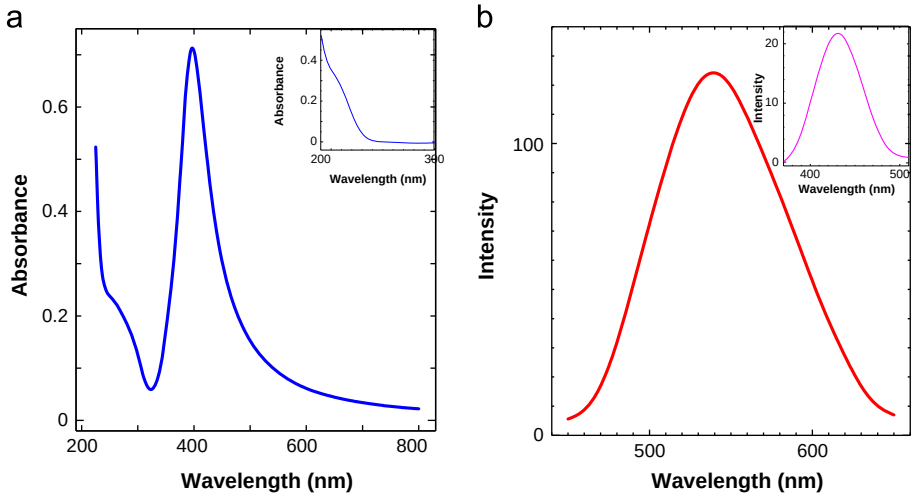

Fig. 1. UV–visible (a) and emission spectra (b) of Chi-AgNPs (λ_{ex}: 394 nm; λ_{em}: 536 nm). Insets: UV–visible (a) and emission spectra of chitosan (λ_{ex}: 210 nm; λ_{em}: 403 nm).

Further, we have studied the emission behavior of chitosan in the presence of malathion. The emission spectrum of chitosan shows the emission maximum at 403 nm while exciting at 210 nm (inset of Fig. 1b). The emission intensity was decreased at 403 nm while adding 1 μM concentration of malathion. Further increasing the concentration of malathion, the emission intensity was dramatically decreased at 403 nm (Fig. S2; Supporting information). The observed spectral changes can be ascribed to the hydrogen bonding interaction between the chitosan and malathion, which leads to a decrease in the absorbance and emission intensities of chitosan. It is expected that more number of malathion molecules will be interacted with chitosan when it was three dimensionally capped with AgNPs and thereby enhance the sensitivity. Thus, we have used chitosan capped AgNPs for the determination of malathion.

3.2. Absorption and emission studies of Chi-AgNPs

When metal nanoparticles were exposed to light, the oscillating electromagnetic field of the light induces a collective coherent oscillation of free electrons (conduction band electrons) of the metal nanoparticles [25,34]. This electron oscillation around the particle surface causes a charge separation with respect to the ionic lattice, forming a dipole oscillation along the direction of the electric field of the light. The amplitude of the oscillation reaches maximum at a specific frequency, called surface plasmon resonance (SPR) [34,35]. The SPR induces a strong absorption of the incident light and thus can be measured using a UV–visible spectrophotometer. The UV–visible spectrum of Chi-AgNPs shows a strong SPR band at 394 nm (Fig. 1a). The stability of the metal nanoparticles can be usually monitored from their absorption characteristics. In contrast to freshly prepared Chi-AgNPs, no change in the absorption characteristics of 6 months aged Chi-AgNPs was observed (Fig. S3; Supporting information). Further, the yellow color of the solution remains the same (inset of Fig. S3; Supporting information). These results indicate that the synthesized Chi-AgNPs were highly stable. The emission spectrum of Chi-AgNPs shows the emission maximum at 536 nm while exciting at 394 nm (Fig. 1b). It depicts a narrow emission profile and half-width full length maximum of 85.7 nm.

Further, we have also synthesized chitosan free AgNPs. They show the absorption maximum at 399 nm with a small hump around 550 nm and the color of the solution is yellow (curve a and inset a of Fig. S4; Supporting information). After 30 min, the absorbance was decreased at 399 nm and the yellow color becomes dark brown (curve b and inset b of Fig. S4; Supporting information). The color of the solution becomes pale green and the absorbance maximum was shifted to 380 nm with decreased absorbance after 1 h, and becomes colorless after 2 h (curve c and inset b Fig. S4; Supporting information). The observed spectral and visible color changes indicate that the AgNPs undergo aggregation due to the absence of a stabilizing agent.

3.3. Determination of Chi-AgNPs concentration and the surface coverage of chitosan ligands

We have estimated the concentration of AgNPs from number of atoms per particles "N" using the following equation [36].

$$N = \pi\rho D^3 N_A / 6M \quad (1)$$

where "ρ" is the density of silver (10.49 g/cm^3), "D" is the average diameter of AgNPs, "N_A" is the Avogadro number (6.023×10^{23}) and "M" is the atomic mass of silver (107.8 g). The concentration of Chi-AgNPs was calculated by using the value of number of atoms per particles "N" [37]:

$$C = N_T / NVN_A \quad (2)$$

where "C" is the concentration of AgNPs, "N_T" is the total number of silver atoms added to $AgNO_3$, and "V" is the volume of the reaction solution in liter. The concentration of Chi-AgNPs was found to be 9.6 μM. Further, we have estimated the surface area of chitosan ligands and it was found to be 1.9 nm^2 [20].

3.4. HR-TEM, XRD, zeta potential and DLS studies

The size and morphology of the Chi-AgNPs were examined by HR-TEM. The HR-TEM images of Chi-AgNPs recorded at different magnifications are shown in Fig. 2. The HR-TEM images illustrate that they are roughly spherical in shape with a size of ~7 nm (Fig. 2A–C). The discrete dots in the diffraction pattern (Fig. 2D) illustrate the crystalline nature of the Chi-AgNPs [39]. Fig. 2C shows the HR-TEM image of single Chi-AgNP. It depicts the lattice images, originating from a single crystal.

The crystalline nature of Chi-AgNPs was also confirmed from the XRD analysis (Fig. S5; Supporting information). It shows the diffraction features appearing at 37.17°, 44.37°, 66.62° and 77.47° corresponding to (111), (200), (220) and (311), respectively [38]. Among the different planes, the peak corresponding to the (111) plane is more intense than the other planes. The ratio between the intensity of the (200) and (111) diffraction peaks was much lower (0.5), suggesting that the (111) plane was a predominant orientation. The width of the (111) peak was employed to calculate the

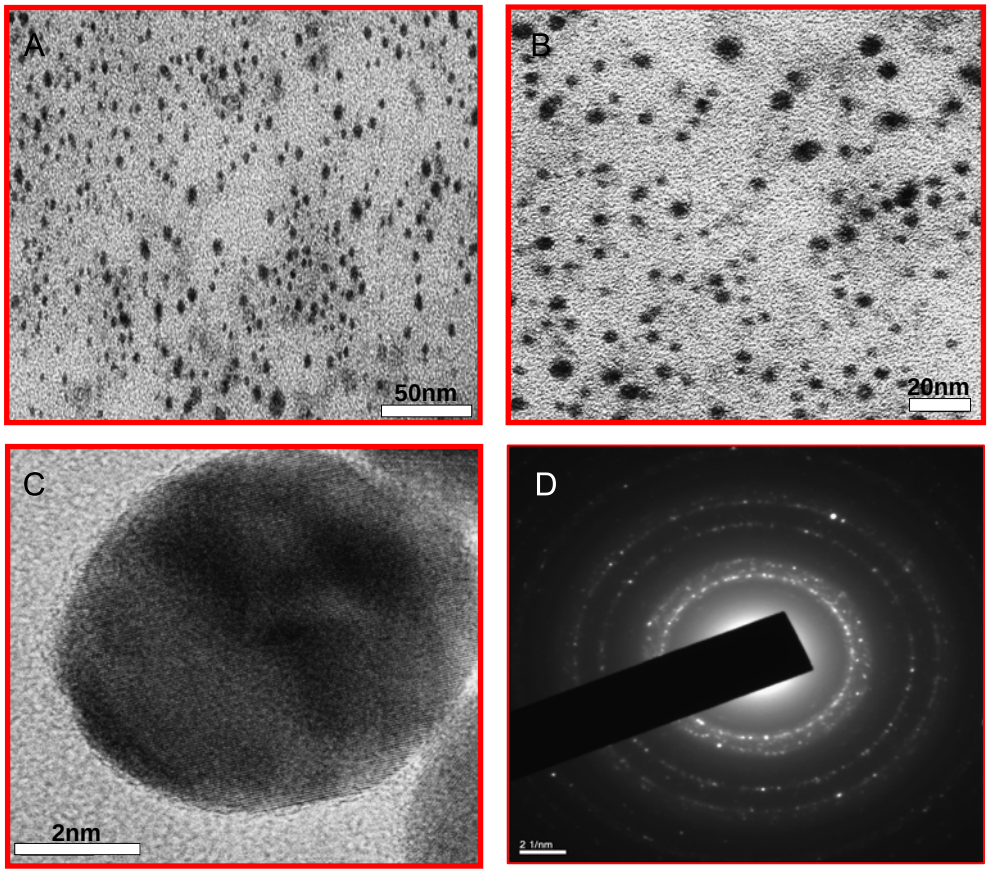

Fig. 2. HR-TEM images of different magnifications (A and B) of Chi-AgNPs, (C) HR-TEM image of single Chi-AgNP and (D) selected area diffraction pattern of Chi-AgNPs.

average crystalline size of the Chi-AgNPs using the Scherrer equation [39]. The calculated average size of the AgNPs is ~8 nm, which fairly matches with the particle size obtained from HR-TEM image.

We have measured the zeta potential of Chi-AgNPs and it was found to be +47.5 mV (Fig. S6(a); Supporting information). The obtained value suggested that the Chi-AgNPs particles having positive charge and the electrostatic repulsion between the positive charges protects the AgNPs from the aggregation (Scheme S1; Supporting information). The DLS of Chi-AgNPs shows that the particle size was ~8 nm (Fig. S6(b); Supporting information). This value closely matches with the particle size obtained from HR-TEM (Fig. 2).

3.5. Determination of band gap energy and ionic strength of Chi-AgNPs

Band gap energy of metal nanoparticles and ionic strength of capped ligands are important to understand the environment of nanoparticles. We have calculated the band gap energy of Chi-AgNPs by using the following equation [40]:

$$\text{Band gap energy } (E) = hC/\lambda \quad (3)$$

where "h" is the Planck constant, "C" is the speed of light and "λ" is the wavelength of absorption maximum.

The band gap energy of Chi-AgNPs was found to be 1.57 eV. The obtained minimum band gap energy suggests the conducting nature of Chi-AgNPs [40].

The ionic strength of Chi-AgNPs was calculated using the following equation [41].

$$\text{Ionic strength } (\mu) = 0.5\ \Sigma c_i z_i^2 \quad (4)$$

where "c_i" is the concentration of the ith species and "z_i" is its charge. The ionic strength of chitosan was found to be 2.28 mM.

3.6. Spectrophotometric determination of malathion

The spectrophotometric method has been extensively used for the determination of biological and toxic chemicals [20,23,38,42]. Therefore, we have attempted to employ this method for the determination of malathion using Chi-AgNPs. Fig. 3 shows the absorption spectra of Chi-AgNPs in the presence of different micromolar concentrations of malathion. The colloidal solution of Chi-AgNPs shows the SPR band at 394 nm (Fig. 3; curve a) and displays a yellow color (Inset (a) of Fig. 3). The SPR band at 394 nm was decreased dramatically and it was also shifted toward higher wavelength while adding micromolar concentration of malathion (curves b–h). Further increasing the concentration of malathion (curves (i–l) of Fig. S7; Supporting information), the absorbance was decreased without affecting the wavelength (Fig. S7; Supporting information (curves (i–l)). The redshift in the SPR band is ascribed to the near-field coupling that occurs when the inter-particle distance decreases. As a result, the AgNPs were aggregated [43–45]. Interestingly, a well defined *isosbestic point* was appeared at 350 nm (Fig. 3) confirming a neat inter-conversion between the dispersed Chi-AgNPs and aggregated Chi-AgNPs. After the addition of 70 μM malathion, an intense yellow color of Chi-AgNPs becomes brown (inset b of Fig. 3). Further increasing the concentration of malathion leads to complete aggregation of AgNPs, which was settled down at the bottom of the quartz cell. The observed spectral and color changes are mainly due to the aggregation of AgNPs. This was confirmed by HR-TEM, DLS and zeta potential studies. The HR-TEM images obtained for Chi-AgNPs after the addition of 70 μM malathion are shown in Fig. 4A and B.

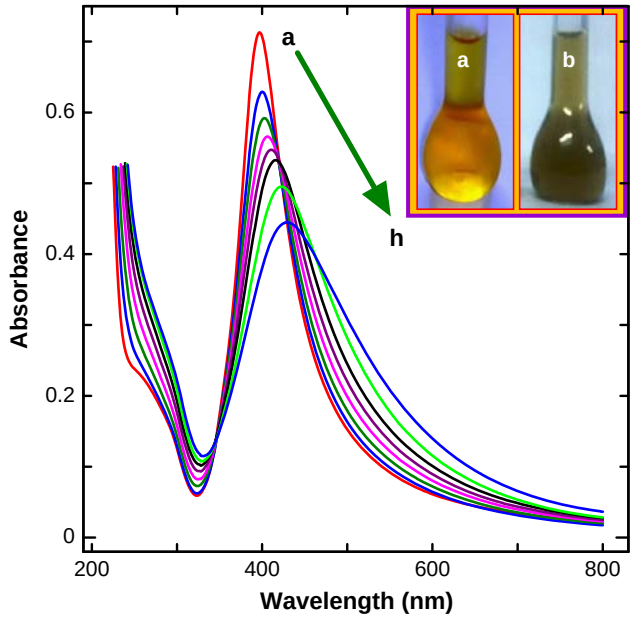

Fig. 3. UV–visible spectra of Chi-AgNPs in the presence of different concentrations of malathion: (a) 0, (b) 10, (c) 20, (d) 30, (e) 40, (f) 50, (g) 60 and (h) 70×10^{-6} M malathion. Inset: Photographic images of (a) before and (b) after the addition of 70 μM malathion into Chi-AgNPs. (For interpretation of the references to color in this figure, the reader is referred to the web version of this article.)

It illustrates the aggregated structure of Chi-AgNPs and the diameter of the aggregated particles is ~150 nm. In contrast to the size of free Chi-AgNPs (Fig. 2), the size of Chi-AgNPs was increased 21-fold in the presence of 70 μM malathion.

According to the Mie theory, when the distance between two nanoparticles becomes smaller than the sum of their radii, the absorbance and emission maximum were decreased [44]. While adding malathion, the Chi-AgNPs were destabilized due to the interaction between Chi-AgNPs and malathion. It leads to a decrease in the distance between the AgNPs. As a result, aggregation of Chi-AgNPs was observed [43–45]. This was further confirmed by zeta potential and DLS measurements. The zeta potential value of Chi-AgNPs after the addition of 70 μM malathion shows −6.04 mV (Fig. S8(a); Supporting information). In contrast to zeta potential value of free Chi-AgNPs, ~8-fold was decreased. Further, the DLS study also confirmed the aggregation of nanoparticles. It shows that the size of the Chi-AgNPs after the addition of 70 μM malathion is 182 nm (Fig. S8(b); Supporting information). It closely matches with the size of the Chi-AgNPs after the addition of 70 μM malathion obtained from HR-TEM (Fig. 4). The absorption spectral response of Chi-AgNPs in the presence of less than micromolar concentrations of malathion do not show any significant changes at 394 nm. Further, no visible color change was observed after the addition of less than micromolar concentrations of malathion to Chi-AgNPs. This suggests that the spectrophotometric method is not suitable to determine less than micromolar concentrations of malathion using Chi-AgNPs. Thus, we have made an attempt to determine malathion by the spectrofluorimetric method.

3.7. Spectrofluorimetric determination of malathion

In order to establish an optimum pH for the determination of malathion, we have studied the emission of Chi-AgNPs in the presence of 10 pM malathion in the pH range of 1.0–10.0 using phosphate buffer solutions. The emission intensity was enhanced from pH 1.0–5.0 and started to decrease beyond pH 5.0 (Fig. S9; Supporting information). It has been reported that the amine group of chitosan will be protonated ($-NH_3^+$) in acidic pH [32,33,46] and this was confirmed by zeta potential measurement. Therefore, we have fixed pH 5.0 for all the experiments.

The fluorescence spectroscopy is an important tool for the determination of toxic chemicals because it posseses high selectivity and sensitivity [19–23]. We have excited both chitosan capped and chitosan free AgNPs at 210 nm. The Chi-AgNPs show a very weak emission band at 403 nm whereas no emission band was observed at 403 nm for the chitosan free AgNPs (inset A of Fig. S5). Since the fluorescence of chitosan was quenched by AgNPs due to the fluorescence resonance energy transfer (FRET) interaction between the chitosan and AgNPs, no emission band was observed for AgNPs. Similar type of quenching has been already reported for different metal nanoparticles capped with various ligands [47–49]. Since excitation of Chi-AgNPs at 210 nm shows a weak emission at 403 nm, we have recorded the emission spectrum of Chi-AgNPs at different excitation wavelengths from 210 to 400 nm (each excitation 2 nm difference). We observed the maximum emission intensity at 536 nm upon excitation at 394 nm. The obtained emission intensity maximum at 536 nm is originated from the SPR of AgNPs. Thus, we have chosen the excitation wavelength of 394 nm for further studies.

Fig. 5 shows the emission spectra of Chi-AgNPs in the presence of different concentrations of malathion. The Chi-AgNPs show the emission maximum at 536 nm with an excitation wavelength of 394 nm (curve a of Fig. 5). Interestingly, even in the presence of 10 pM malathion, the emission intensity of Chi-AgNPs at 536 nm was decreased and the emission maximum was shifted toward higher wavelength (Fig. 5; curve b). Further increasing the concentrations of malathion, the emission intensity at 536 nm was dramatically decreased (Fig. 5; curves b–l). In contrast to Chi-AgNPs (Fig. 5; curve a), emission intensity was decreased 8-fold while adding 140 pM concentration of malathion (Fig. 5; curve o). The observed decrease in emission intensity and redshift of emission wavelength are mainly due to the aggregation of Chi-AgNPs. A good linearity was observed in the emission intensity against 1×10^{-9}–10×10^{-12} M malathion (R^2=0.9968) (inset of Fig. 5) and the detection limit was found to be 94 fM L^{-1} (S/N=3).

3.8. Mechanism for the aggregation of Chi-AgNPs

Hydrolysis of malathion in acidic pH can dissociate into two forms such as dimethyl phosphorothionic acid and 2-mercaptodiethylsuccinic acid (Chart 1) [8]. The acidic –OH group of 2-mercaptodiethylsuccinic acid has the hydrogen bonding interaction with –OH group of chitosan [50]. Moreover, hydrogen bonding interaction will be expected between –OH group of phosphorothionic acid and –OH group of chitosan (Fig. 4B) [46,50]. These hydrogen bonding interactions lead to a decrease in both the absorbance and emission intensities of Chi-AgNPs as a result of aggregation.

3.9. Reproducibility

We have tested the reproducibility for the determination of malathion by both spectrophotometry and spectrofluorimetry. We have determined the malathion using both freshly prepared AgNPs and 1 and 2 months aged Chi-AgNPs. The corresponding results are shown in Fig. S10A and B (Supporting information). Both UV–visible and emission spectra exhibit good reproducibility (Fig. S10A and B; Supporting information), indicating that the proposed method has high precision and accuracy.

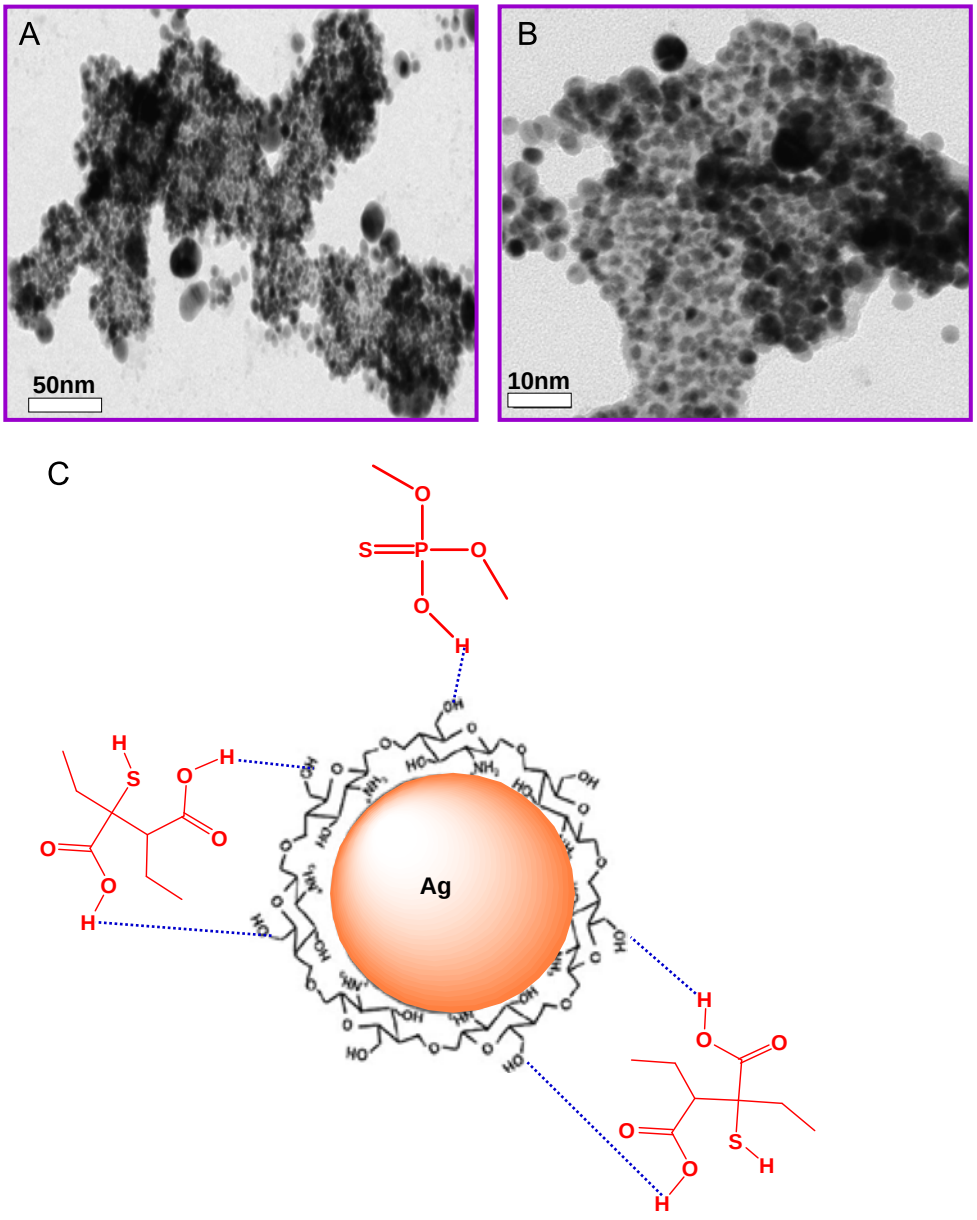

Fig. 4. (A and B) HR-TEM images of different magnifications of Chi-AgNPs in the presence of 70×10^{-6} M malathion. (C) Schematic representation for the possible interaction between Chi-AgNPs and malathion at pH 5.

3.10. Determination of quantum yield and binding constant

The determination of quantum yield is generally accomplished by a comparison of the wavelength–integrated intensity of the unknown sample with the standard. Fluorescent quantum yield values (ϕ_F) of Chi-AgNPs in the presence and absence of malathion were calculated by using the comparative William's method [51]. For this purpose, we used quinine sulfate as reference quantum yield standard. The integrated fluorescence intensities of Chi-AgNPs and malathion aggregated Chi-AgNPs were plotted versus absorbance for the reference standard. The gradients of the plot are proportional to the quantity of quantum yield of the standard molecules. The ϕ_F value was calculated according to Eq. (1).

$$\varphi_{F(X)} = (\mathrm{Grad}_X/\mathrm{Grad}_{ST})(n^2{}_X/n^2{}_{ST}) \quad (5)$$

where "ST" and "X" denote standard and sample, respectively. "Grad" is the gradient from the plot and "n" is the refractive index of the solvent (water). According to the data, fluorescence quantum yield values of Chi-AgNPs and malathion aggregated Chi-AgNPs were found to be 0.6394 and 0.1582, respectively. The obtained high quantum yield value suggests the high fluorescence nature of AgNPs. The addition of malathion to Chi-AgNPs decreases the emission intensity due to aggregation of AgNPs and thereby the quantum yield was decreased 4-fold.

The binding constant (K_A) value can be estimated by using the following equation [52].

$$\log [F-F_0/F_0] = \log K_A + n \log [Q] \quad (6)$$

where, "F_0" is the fluorescence intensity of Chi-AgNPs and "F" is the fluorescence intensity of Chi-AgNPs in the presence of malathion. "K_A" is the binding constant, "n" is the number of binding sites and "Q" is the concentration of malathion. K_A and n can be measured from the intercept and slope obtained through plotting $\log[F-F_0/F_0]$ against $\log[Q]$ (Fig. S11; Supporting information). The binding constant (K_A) was found to be $K_A = 4.9980 \times 10^{10}$ mol^{-1} L. The obtained binding constant value suggests that there is a strong binding force between malathion and Chi-AgNPs.

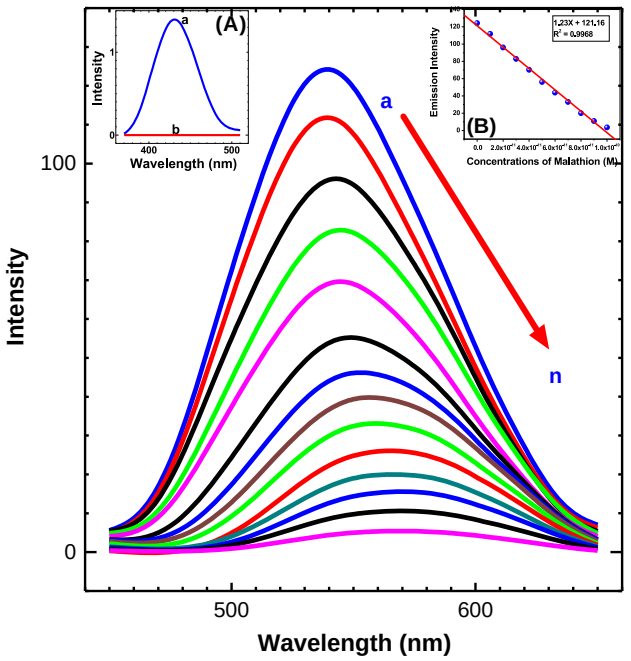

Fig. 5. Emission spectra of Chi-AgNPs in the presence of different concentrations of malathion: (a) 0, (b) 10, (c) 20, (d) 30, (e) 40, (f) 50, (g) 60, (h) 70, (i) 80, (j) 90, (k) 100, (l) 110, (m) 120, (n) 130 and (o) 140×10^{-12} M malathion (λ_{ex}: 394 nm; λ_{em}: 536 nm). Inset (A): Emission spectrum of (a) chitosan capped AgNPs and (b) chitosan free AgNPs (λ_{ex}:210 nm; λ_{em}: 536 nm). Inset (B): calibration plot for decrease in emission intensity against concentration of malathion.

3.11. Quenching mechanism, Stern–Volmer and association constant

The quenching constant (K_{SV}) can be calculated by the Stern–Volmer equation [53].

$$F_0/F = 1 + K_{SV}[Q] \quad (7)$$

where "F" is the fluorescence intensity of Chi-AgNPs in the presence of malathion and "F_0" is the fluorescence intensity of dispersed Chi-AgNPs. "K_{SV}" is the Stern–Volmer quenching constant and "[Q]" is the concentration of malathion. The Stern–Volmer plot F_0/F versus [Q] showed a positive deviation (Fig. S12; Supporting information). The obtained Stern–Volmer plot is linear and K_{SV} was found to be 6.05×10^{11} L mol^{-1}. The positive deviation was observed at higher concentrations of malathion. This may be due to the simultaneous presence of dynamic and static quenching [53,54]. The obtained Stern–Volmer constant value suggests the presence of strong fluorescence quenching between Chi-AgNPs and malathion.

The fraction of malathion bound to the Chi-AgNPs (θ) was determined by the following equation [55]:

$$\theta = F_0 - F/F_0 \quad (8)$$

From the value of "θ", the association constant K_f can be calculated with the help of the following equation [56].

$$(1/1-\theta)\, K_f = [\text{Malathion}]/\theta - n[\text{AgNPs}] \quad (9)$$

where "n" is the number of binding sites, [malathion] is the concentration of malathion and [AgNPs] is the concentration of Chi-AgNPs. From the plot of $1/(1-\theta)$ versus [malathion]/θ, the value of K_f was calculated. It was found to be 3.85×10^{12} mol L^{-1}. The standard Gibbs free energy change (ΔG^0 was calculated from the K_f using the relation $\Delta G^0 = -2.303RT \log_{10} K_f$) was found to be −51 kJ. The obtained negative value of Gibbs free energy change indicates that the interactions between malathion and Chi-AgNPs were spontaneous.

3.12. Effect of interferences

The determination of 10 nM malathion in the presence of 1000-fold higher concentrations of common interferences, imidacloprid, endosulfan, methyl parathion, alphamethrin and chloropyrifos was studied (Fig. S13; Supporting information). The emission spectra of Chi-AgNPs in the presence of imidacloprid, endosulfan, methyl parathion, alphamethrin and chloropyrifos (Fig. S13B; Supporting information; curves b–f) do not alter the emission spectrum of Chi-AgNPs (curve a), However, while adding 10 nM malathion into this solution containing the interferences, the emission intensity was decreased and the emission maximum was shifted to higher wavelength (Fig. S13B; Supporting information; curve g). These results confirmed that the Chi-AgNPs showed high selectivity toward malathion (Fig. S13A and B; Supporting information). To the best of our knowledge, this is the first report with high sensitivity and selectivity for the determination of malathion using Chi-AgNPs by spectrofluorimetry method in an aqueous medium.

3.13. Real sample analysis

We have determined malathion in polluted lake water and fruit samples such as grapes and mangos. The fruit samples were pretreated by using the method given in the section 2. Different concentrations of malathion were added into real samples and the emission spectra of Chi-AgNPs were recorded. Table 1 shows the recoveries of 99.8% and 101.2% and good agreement was observed between the spiked and measured malathion. The results obtained by the present method fairly matched with the results obtained from the HPLC method (Table 2). On the basis of T-test and F-test, the results obtained from our present approach are in good consensus with the results obtained by the HPLC method.

4. Conclusions

In the present study, we have used Chi-AgNPs fluorophore for the determination of malathion in lake water and fruit samples. The emission intensity of Chi-AgNPs was decreased at 536 nm (λ_{ex}: 394 nm) with redshift. Based on the decrease in emission intensity, the concentration of malathion was determined. The lowest detection limit was found to be 94 fM L^{-1}. The presence of 1000-fold common interferences such as chloropyrifos, methyl parathion, endosulfon, imidacloprid and alphamethrin do not interfere in the determination of 10 nM malathion. The proposed method was successfully applied for the determination of malathion in water and fruit samples. Further, the results obtained from the

Table 1
Recovery test for malathion in lake water, mangos and grapes samples.

Samples	Malathion added (ng L^{-1})	Malathion found (ng L^{-1})	RSD	Recovery (%)
Polluted lake water	–	10.13 ± 0.10	0.95	–
	10	20.16 ± 0.03	0.99	99.8
	20	30. 78 ± 0.05	1.03	101.2
Mangos	–	–	–	–
	10	10.01 ± 0.03	1.12	100.3
	20	20.02 ± 0.04	1.05	100.3
Grapes	–	–	–	–
	10	9.97 ± 0. 01	0.86	99.8
	20	20.01 ± 0.04	1.10	100.3

Table 2
Comparison of the present method of malathion determination with the HPLC method.

Malathion spiked (mg L^{-1})	Malathion measured (mg L^{-1})		RSD (%) ($n=5$)	*T*-test	*F*-test
	Fluorimetry method (this work)	HPLC method			
0.01	0.01 ± 02	0.014 ± 04	99.8	0.2756	1.0
0.02	0.02 ± 01	0.025 ± 01	100.1	0.3215	1.0

present method were validated with the HPLC method. To the best of our knowledge, this is the first report with high selectivity and low detection limit for malathion than any other methods.

Acknowledgments

Mr. N. Vasimalai thanks the Council of Science Industrial Research (CSIR), New Delhi, for the award of Senior Research Fellow 09/715(0017)/2012-EMR-I. We acknowledge the financial support from the University Grants Commission (42-283/2013 (SR)), New Delhi. We also thank Dr. S. Meenakshi, Department of Chemistry, Gandhigram Rural Institute, Gandhigram, for providing chitosan and Dr. A. Siva, School of Chemistry, Madurai Kamaraj University, Madurai, for HPLC measurements. The authors are grateful to PSG Institute of Advanced Studies, Coimbatore, for HR-TEM measurements.

Appendix A. Supporting information

Supplementary data associated with this article can be found in the online version at http://dx.doi.org/10.1016/j.talanta.2013.04.033.

References

[1] A. Scheyer, O. Briand, S. Morville, P. Mirasel, Anal. Bioanal. Chem. 387 (2007) 359–368.
[2] F. Arduini, F. Ricci, C.S. Tuta, D. Moscone, A. Amine, G. Palleschi, Anal. Chim. Acta. 580 (2006) 155–162.
[3] K. Tuovinen, M. Kolehmainen, H. Paakkanen, Anal. Chim. Acta. 429 (2001) 257–268.
[4] T.-J. Lin, K.-T. Huang, C.-Y. Liu, Biosens. Bioelectron. 22 (2006) 513–518.
[5] M.S. Bootharaju, T. Pradeep, Langmuir 28 (2012) 2671–2679.
[6] N.E. Barlas, Bull. Environ. Contam. Toxicol. 57 (1996) 705–712.
[7] L. Mccarroll, M.G. Paton, S.H. Karunaratne, H.T. Jayasuriya, K.S. Kalpage, J. Hemingway, Nature 407 (2000) 961–962.
[8] ⟨http://www.swrcb.ca.gov/rwqcb5/water_issues/tmdl/central_valley_projects/central_valley_pesticides/criteria_method/malathion/final_malathion_criteria_rpt.pdf⟩.
[9] D. Liu, W. Chen, J. Wei, X. Li, Z. Wang, X. Jiang, Anal. Chem. 84 (2012) 4185–4191.
[10] ⟨http://www.nvbdcp.gov.in⟩.
[11] R.K. Albright, B.W. Kram, R.P. White, J. Am. Med. Assoc. 250 (1983) 2469–2470.
[12] P.D. Moore, A.K. Patlolla, P.B. Tchounwou, Mutat. Res. 725 (2011) 78–82.
[13] X.-Y. Chen, J.-Z. Shao, L.-X. Xiang, X.-M. Liu, Comp. Biochem. Phys. C 142 (2006) 36–45.
[14] W. Aqel A-Qare, B. Mohamed A-Donia, J. Pharmaceut. Biomed. 26 (2001) 291–299.
[15] Y.W. Lin, S.S.Q. Hee, J. Chromatogr. A 814 (1998) 181–186.
[16] N. Chauhan, C.S. Pundir, Anal. Chim. Acta 701 (2011) 66–74.
[17] G. Quintas, A. M-Noe, S. Armenta, S. Garrigues, M. de la Guardia, Anal. Chim. Acta 502 (2004) 213–220.
[18] G. Quintas, Sa. Garrigues, M. de la Guardia, Talanta 63 (2004) 345–350.
[19] K.R. Mohan, A. Ramesh, K. Seshaih, Analyst 125 (2000) 323–326.
[20] N. Vasimalai, S.A. John, Biosens. Bioelectron. 42 (2013) 267–272.
[21] D. Mazumdar, J. Liu, G. Lu, J. Zhou, Y. Lu, Chem. Commun. 46 (2010) 1416–1418.
[22] N. Vasimalai, S.A. John, Analyst 137 (2012) 3349–3354.
[23] C.-I. Wanga, C.-C. Huangb, Y.-W. Linc, W.-T. Chena, H.-T. Chang, Anal. Chim. Acta 745 (2012) 124–130.
[24] Z.D. Wang, Y. Lu, J. Mater. Chem. 19 (2009) 1788–1798.
[25] A.S. Nair, R.T. Tom, T. Pradeep, J. Environ. Monitor. 5 (2003) 363–365.
[26] R.K. Bera, A.K. Das, C.R. Raj, Chem. Mater. 22 (2010) 4505–4511.
[27] B. Adhikari, A. Banerjee, Chem. Mater. 22 (2010) 4364–4371.
[28] J. Zhang, X. Li, X. Sun, Y. Li, J. Phys. Chem. B 109 (2005) 12544–12548.
[29] Y. Wang, F. Yang, X. Yang, ACS Appl. Mater. Interfaces 2 (2010) 339–342.
[30] M.N.V. Ravi Kumar, React. Funct. Polym. 46 (2000) 1–27.
[31] C.K.S. Pillai, W. Paul, C.P. Sharma, Prog. Polym. Sci. 34 (2009) 641–678.
[32] M. Dash, F. Chiellini, R.M. Ottenbrite, E. Chiellini, Prog. Polym. Sci. 36 (2011) 981–1014.
[33] G.N. Kousalya, M. Rajiv Gandhi, C. Sairam Sundaram, S. Meenakshi, Carbohyd. Polym. 82 (2010) 594–599.
[34] M.-C. Daniel, D. Astruc, Chem. Rev. 104 (2004) 293–346.
[35] K.-S. Lee, M.A. El-Sayed, J. Phys. Chem. B 110 (2006) 19220–19225.
[36] R.T. Tom, V. Suryanarayanan, P.G. Reddy, S. Baskaran, T. Pradeep, Langmuir 20 (2004) 1909–1914.
[37] ⟨http://www.cristalvillage.org/NPs%20calc.htm⟩.
[38] N. Vasimalai, S.A. John, J. Hazard. Mater. 213–214 (2012) 193–199.
[39] B.D. Cullity, Elements of X-ray Diffraction, 2nd Ed., Addision-Wesley, Menlo Park, CA, 1978.
[40] M. Hoffman, S. Martin, W. Choi, D. Bahnemann, Chem. Rev. 95 (1995) 69–96.
[41] A.A. Volkert, S. Varuni, A.J. Haes, Chem. Commun. 47 (2011) 478–480.
[42] Y. Yao, D. Tian, H. Li, ACS Appl. Mater. Interfaces 2 (2010) 684–690.
[43] K.-H. Su, Q.-H. Wei, X. Zhang, J.J. Mock, D.R. Smith, S. Schultz, Nano Lett. 3 (2003) 1087–1090.
[44] G. Mie, Ann. Phys. 330 (1908) 377–445.
[45] B.K. Jena, C.R. Raj, Biosens. Bioelectron. 23 (2008) 1285–1290.
[46] D.R. Bhumkar, H.M. Joshi, M. Sastry, V.B. Pokharkar, Pharmaceut. Res. 24 (2007) 1415–1426.
[47] C.Y. Wang, C.Y. Liu, X.B. Yan, J.J. He, M.H. Zhang, T. Shen, J. Photochem. Photobiol. A 104 (1997) 159–164.
[48] S. Link, M.A. El-Sayed, Int. Rev. Phys. Chem. 19 (2000) 409–453.
[49] M.M.Y. Chen, A. Katz, Langmuir 18 (2002) 2413–2420.
[50] Thomas Steiner, Angew. Chem. Int. Ed. 41 (2002) 48–76.
[51] A.T.R. Williams, S.A. Winfield, J.N. Miller, Analyst 108 (1983) 106–108.
[52] J. Gao, Y. Guo, J. Wang, Z. Wang, Z. Jin, C. Cheng, Y. Li, K. Li, Spectrochim. Acta A 78 (2011) 1278–1286.
[53] J.S. Park, J.N. Wilson, K.I. Hardcastle, U.H.F. Burnz, M. Srinivasarao, J. Am. Chem. Soc. 128 (2006) 7714–7715.
[54] Q. Zhou, T.M. Swager, J. Am. Chem. Soc. 117 (1995) 12593–12602.
[55] G. Weber, L.B. Young, J. Biol. Chem. 239 (1964) 1415–1423.
[56] L.D. Ward, Enzymology 117 (1985) 400–414.